Physicochem. Probl. Miner. Process., 61(4), 2025, 204869 | Physicochemical Problems of Mineral Processing

http://www.journalssystem.com/ppmp | ISSN 1643-1049
© Wroclaw University of Science and Technology

Study of gas parameters within the mineralized bed of fluidized bed flotation column

Ning Han, Yanfeng Li

State Key Laboratory of Coking Coal Resources Green Exploitation, China University of Mining and Technology, Xuzhou 221116, China

School of Chemical Engineering and Technology, China University of Mining and Technology, Xuzhou 221116, Jiangsu, China

Corresponding author: lyf3344@126.com (Yanfeng Li)

Abstract: Accurate resolution of gas dispersion parameters in multiphase flow is crucial for optimizing the performance of fluidized bed flotation. In this study, a gas-liquid-solid three-phase system consisting of compressed air, water, and steel beads was constructed, and the effects of apparent water velocity, apparent gas velocity, static bed layer height, and heavy-phase mass ratio on the bubble diameter and gas content were systematically investigated. The results showed that the minimum value of bubble diameter was 0.56 mm and the maximum value of gas content was 0.1835 at a static bed height of 0.2885 m and a heavy-phase mass ratio of 50%, and a four-factor, three-level mathematical model was further developed by Box-Behnken response surface design, and the analysis showed that the static bed height and the apparent water velocity were the main factors affecting the bubble diameter, with a significance of $p<0.05$. Finally, the effects of bubble diameter and gas content were established. 0.05. Finally, a prediction model between bubble diameter and multiple factors was established to provide theoretical support for the structural design and industrial application of three phase fluidized bed flotation columns.

Keywords: flotation, fluid, bubble diameter, gas content, mineralization

1. Introduction

In this study, gas-liquid-solid three phase fluidized bed flotation columns are characterized as systems where solid particles are kept in suspension by an upward stream of compressed air. This air functions as the dispersed gaseous phase, while water constitutes the continuous liquid medium. Reese et al. (Jo et al., 2022) investigated practical implementations of such three-phase systems in industrial contexts, highlighting their advantages. These fluidized beds have been extensively applied in scientific research across chemistry, physics, and biochemistry (Abu et al., 2021; Jena et al., 2008b). Since their introduction, flotation columns have undergone considerable development, largely due to their flexibility in treating fine particles and their use across diverse scientific disciplines (Bhunia et al., 2015; Cai et al., 2017; Fan et al., 2013; Lei et al., 2020; Venkatraman, 1996). Parameters related to the gas phase, including gas hold-up, bubble diameter (D_b), and bubble surface area flux, are key determinants of flotation effectiveness, directly influencing the operation of flotation columns (Li et al., 2008; Vadlakonda et al., 2018).

A detailed comprehension of gas-related parameters is vital for the operational control and analysis of flotation columns. The literature has presented a broad range of studies examining such parameters (Jena et al., 2008a; Lefebvre et al., 2007; Sobrino et al., 2009; Wang et al., 2003). Research on gas-phase behavior in flotation systems dates back to the late 20th century, with Yianatos employing impulse response techniques to study the residence time distribution of radioactive gas tracers (Yianatos et al., 2017). Later, Ityokumbul suggested a direct method for estimating bubble sizes in flotation columns (Pan et al., 2018). Gorain proposed an empirical approach to quantify bubble surface area flux in mechanical flotation cells, derived from large-scale pilot studies (Gorain et al., 1999). Sarhan developed a computational fluid dynamics (CFD) model to simulate gas hold-up and bubble behavior in three-

DOI: 10.37190/ppmp/204869

phase flotation columns (Sarhan et al., 2017), while Wang also utilized CFD to simulate and analyze the flotation process in depth (Wang et al., 2018). Ravichandran focused on refining gas-phase conditions to improve gas hold-up and thereby enhance flotation outcomes (Ravichandran et al., 2013). Despite these advancements, an integrated analysis of fundamental gas-phase metrics such as D_b, gas hold-up, and surface area flux in the context of flotation columns remains limited.

Bubble shape is primarily influenced by five core physical characteristics: diameter, velocity, density, viscosity, and surface tension. To describe these shapes, dimensionless numbers such as the Eötvös (Eo), Weber (We), Reynolds (Re), and Morton (Mo) numbers are commonly employed (Ellingsen et al., 2001; Liu et al., 2021). One of the most straightforward indicators of bubble shape is the aspect ratio—defined as the ratio of the minor axis to the major axis of the bubble. In recent years, numerous studies have investigated individual bubble morphologies. Experimental data suggest that these dimensionless parameters effectively capture the nuances of bubble shape (Aoyama et al., 2016; Shi et al., 2018). However, Loth (Loth, 2008) highlighted that findings based on single-bubble studies may not translate well to multiphase or two-phase flows, as interactions among bubbles, liquid motion, and phase properties can considerably modify the observed shapes. Liu (Liu et al., 2021) discovered that, contrary to single-bubble theory, bubble aspect ratios tend to level off with increasing bubble size, instead of showing an inverse relationship with D_b. Besagni (Besagni et al., 2019) underscored the importance of correlating bubble shape in multi-bubble systems with specific process conditions.

This study explores the application of a three-phase fluidized bed system as an innovative flotation column for mineral separation. A significant feature of this system is the inclusion of turbulence-regulated particles, which facilitate the collision and attachment of flotation particles to bubbles. The behavior of bubbles plays a central role in the mineralization process, emphasizing the necessity of examining gas parameters within the mineralized zone of the fluidized bed flotation column. The research aimed to assess how variables—such as static bed height, the presence of steel balls, the mass ratio of the dense phase, and apparent velocities of both water and gas—affect D_b and gas content. These findings are expected to support optimization of gas-related parameters in mineral flotation, promote the advancement of three phase fluidized bed flotation column technologies, and lay groundwork for future system development and theoretical modeling.

2. Materials and methods

2.1. Principles of equipment

As depicted in Fig. 1, the fluidized bed flotation column can be divided into three key sections based on

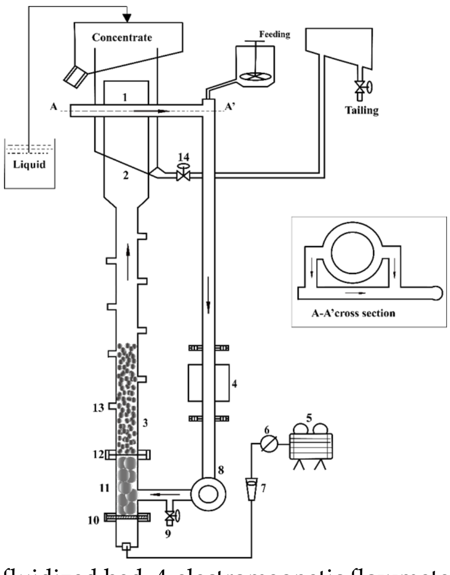

1-circulation pipe; 2-buffer; 3-fluidized bed; 4-electromagnetic flowmeter; 5-air compressor; 6-gas valve; 7-rotor flowmeter; 8-circulation pump; 9-unloading port; 10-gas distributor (fluidized plate); 11-mixing bed; 12-screen plate; 13-pressure measuring hole; 14-valve.

Fig. 1. Schematic diagram of three phase fluidized bed flotation column

its operational principle: the mineralization section, the froth selection area, and the medium ore circulation system. These sections are interconnected, and their working principles are as follows: the upward water flow interacts with the particles in the mineralization and fluidization section. This interaction causes the particles to gradually fluidize, forming a fluidized bed layer with specific turbulence intensity and porosity. And at the same time, the gas produced by the gas compressor is turned into bubbles of certain diameters under the cutting of the gas distributor (ceramic plate) at the bottom of the column body and arrives at the fluidized bed layer, and the stirred slurry is fed into it from the top of the column. After stirring, the slurry is fed from the top of the flotation column, and then pumped into the bottom of the column with the circulating water flow under the action of the circulating pump. The rising flotation particles meet with the bubbles in the fluidized bed layer, and then collide and mineralize by the joint action of the rising water flow and turbulence-controlled particles, the turbulence intensity of the fluidized bed layer is changed through the adjustment of the apparent water velocity and the nature of the filled particles, and the flotation particles with different particle sizes are fully mineralized, and the mineralized particles are extended by the column flotation section of a larger cross-sectional area. These mineralized particles are fully mineralized, and these mineralized particles pass through the column flotation section with larger cross-sectional area and prolong the flotation time, and finally obtain the flotation concentrate, which is a kind of flotation process separating mineralization and flotation.

2.2. Bubble data acquisition system

2.2.1. Introduction to the instrument

In this study, bubble characteristic data in the three-phase fluidized bed were collected using a data acquisition system comprising a BVW-2 conductivity probe bubble measurement device connected to a computer. A schematic representation of the measurement setup is provided in Fig. 2.

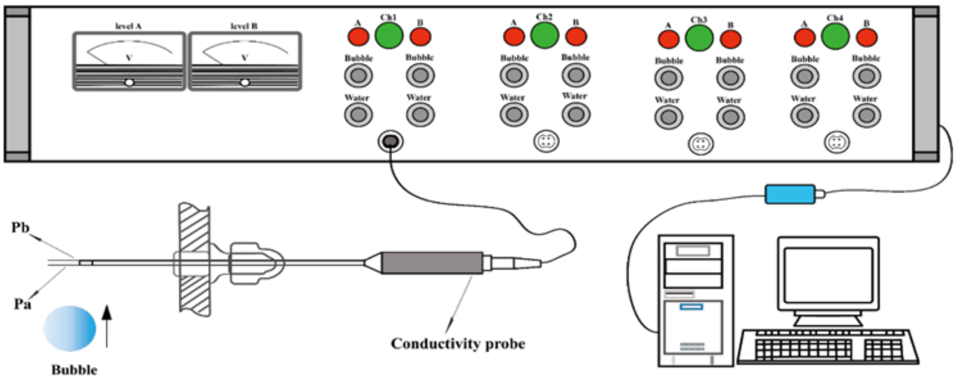

Fig. 2. Measuring device BVW - 2 for bubble characteristics

Prior to measuring the bubble characteristics in the three-phase fluidized bed flotation column, the conductivity probe is inserted into the central cross-section of the column through the designated pressure port. The experimental system is initiated following a water leakage prevention procedure. Once a stable gas-liquid-solid three-phase flow is established within the fluidized bed, data collection begins. A schematic diagram illustrating the experimental setup and operation is presented in Fig. 3. It is important to ensure that probes P*a* and P*b* are aligned along the direction of bubble movement. When a bubble simultaneously contacts both probes, the conductivity readings of P*a* and P*b* change accordingly, resulting in a corresponding voltage fluctuation curve.

In multiphase flow systems, because of the variability of bubble size, the size of D_b is generally represented by the average D_b of the bubble characteristics under a certain experimental condition. For a group of bubbles, the average diameter of a group of bubbles is generally represented by the Sauter diameter, the average diameter of the Sauter is represented by d_{32}, then d_{32} can be calculated by equation 1, the BVW-2 bubble measurement equipment used in this study is the average diameter of the bubble Sauter calculated. After the computer converts the signal from the probe into a voltage value, the relevant software performs a series of calculations on the voltage value to finally calculate the bubble Sauter diameter.

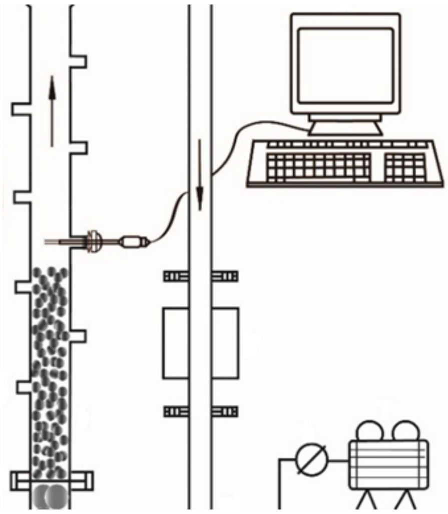

Fig. 3. Schematic diagram of bubble measurement

$$d_{32} = \frac{\sum n_i d_{bi}^3}{\sum n_i d_{bi}^2} \tag{1}$$

2.3. Test characterization parameters

2.3.1. Apparent water velocity

The apparent water velocity is the ratio of the liquid flow rate to the cross-sectional area of the column in the mineralized section and is calculated as follows:

$$V_l = \frac{Q_l}{A} \tag{2}$$

where: Q_l - liquid flow rate, m^3/s; A - cross-sectional area of the column in the mineralized section, m^2.

2.3.2. Apparent gas velocity

The apparent gas velocity is the ratio of the gas flow rate to the cross-sectional area of the column and is calculated as follows:

$$V_g = \frac{Q_g}{A} \tag{3}$$

where: Q_g - gas flow rate, m^3/s; A - cross-sectional area of column in mineralized section, m^2.

2.3.3. Gas content ratio

The gas content is the volume percentage of the gas in the three-phase or two-phase, and the corresponding gas content is calculated using the differential pressure method with the following formula:

$$\frac{P_2 - P_1}{\Delta H \cdot g} = \rho_l \cdot \varepsilon_l + \rho_g \cdot \varepsilon_g + \rho_s \cdot \varepsilon_s \tag{4}$$

$$\varepsilon_l + \varepsilon_g + \varepsilon_s = 1 \tag{5}$$

$$\varepsilon_s = \frac{M_S}{A \cdot H} \tag{6}$$

The formula for gas content ratio is obtained by generalization:

$$\varepsilon_g = \frac{(P_2 - P_1)/(\Delta H \cdot g) - \rho_l + \varepsilon_s \cdot (\rho_l - \rho_s)}{\rho_g - \rho_l} \tag{7}$$

where: P_2, P_1 - pressure at the pressure measurement hole, kPa; ΔH - pressure measurement hole spacing, m; g - gravitational acceleration; ρ_l - fluid density, kg/m^3;ε_s - solids content; ρ_s - Solid density, kg/m^3; ρ_g - gas density, kg/m^3.

3. Results and discussion

3.1. Measurement and analysis of bubble diameter research

3.1.1. Study of the effect of static bed layer height on bubble diameter

Fig. 4 shows the trend of D_b exhibited with the change of static bed layer height at different apparent air velocities when the mass ratio of steel ball heavy phase (diameter 5 mm) is 50% and the apparent water velocity is 0.2265 m/s. When the apparent air velocity is constant, D_b decreases and then increases with the increase of the static bed layer height, and there is a minimum value of D_b when the static bed layer height is 0.2885m. This is because the bed steel beads in the rising water flow under the action of fluidization, filled steel beads to obtain kinetic energy and irregular mutual collision, the rising bubble shear effect, the rising bubble tail vortex and exacerbate the movement of the steel beads, static bed layer height increase makes the steel beads on the bubble shear also enhanced, while the bubble through the mineralized bed layer time is also lengthened, resulting in the bubble fragmentation and make the diameter decrease, with the static bed layer height further increase, the steel bead shear diameter of the bubble has the minimum. With the further increase of the static bed height, the shear effect of steel ball gradually reaches the optimum, and after the bed height is higher, the retention time of the bubbles in the bed is too long, which leads to the merger of bubbles in the process of ascending, so the diameter of the bubbles becomes larger. It can also be seen that, in the static bed layer height is lower than 0.2885m, the difference of At the heavy phase mass ratio of 50% under the four apparent gas velocity is larger, this is because the static bed layer height is lower, the bed layer steel ball on the bubble of the shear effect is limited, the bubble in the bed layer retention time is shorter, therefore, the apparent gas velocity increases, the bubble can not be sufficiently broken by the shear, the D_b is relatively larger. On the contrary, at higher bed heights, it can be seen that there is little difference in D_b under the four apparent gas velocities, which fully demonstrates that the static bed height not only has a shearing effect on the bubbles, but also has a strong merging effect, and also shows from the side that the static bed height has a more pronounced homogenizing effect on bubbles with higher gas velocities.

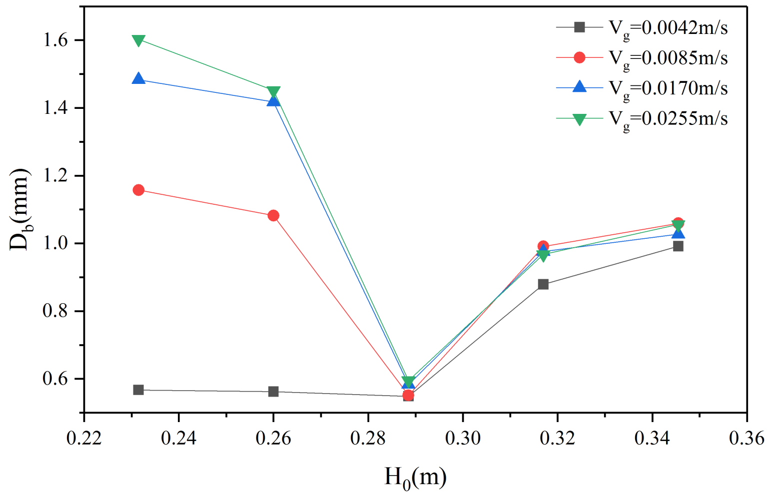

Fig. 4. Relationship between Db and static bed height

3.1.2. Study of the effect of heavy phase mass ratio on bubble diameter

Fig. 5 presents the effect on D_b due to different heavy phase mass ratios at four apparent gas velocities: 0.0042 m/s, 0.0085 m/s, 0.0170 m/s, and 0.0255 m/s when the apparent water velocity is 0.2265 m/s and the static bed height is 0.2885 m. D_b is also affected by the heavy phase mass ratio. From the figure, it can be seen that under the same apparent gas velocity condition, D_b has a tendency to decrease and then increase with the increase of the heavy phase mass ratio. This is because the addition of the heavy phase makes the particle size ratio of the same column cross-section in the column increase, the two particle size steel beads are mixed more closely, filling each other's fluidization gap, and the difference in particle size on the column cross-section reaches the maximum when the mass ratio of the heavy phase is 50%, the bed has the strongest shear effect on the bubbles, and at this time D_b is the smallest. It can also be seen that for higher gas velocities, D_b at a heavy phase mass ratio of 100% is slightly smaller than that at 0%, while for lower gas velocities, the opposite is true. This is because the heavy-phase mass ratio of 0%, that is, all light-phase steel beads, the gas velocity increases, the synergistic effect with the liquid phase is enhanced, increasing the liquid-phase turbulence intensity, this time the steel beads are lighter, the bed porosity increases , the bed steel beads of the shear effect becomes weaker, while for the heavy-phase mass ratio of 100%, this time the liquid-phase turbulence intensity of the heavy-phase beads of the shear effect strengthens the shear action of the steel beads of the steel beads of the steel beads of the shear effect is strong, D_b is small, therefore At higher gas velocities, the heavy-phase mass ratio of 100% is slightly smaller than D_b at 0%, and similarly, the opposite conclusion is reached at lower gas velocities.

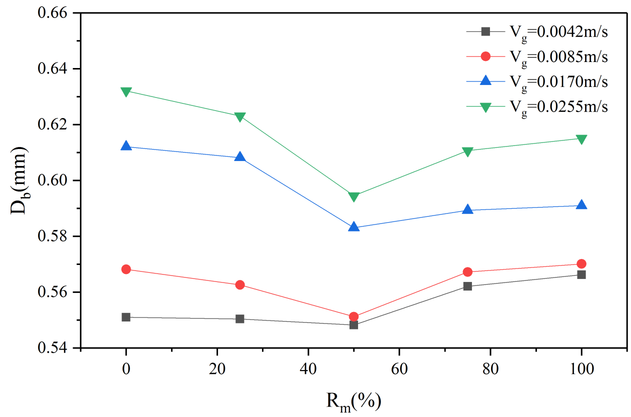

Fig. 5. Relationship between D_b and heavy mass rate

3.1.3. Study of the effect of apparent water velocity on bubble diameter

As shown in Fig. 6, D_b initially declines, then rises, and eventually plateaus with increasing apparent water velocity. Among the four tested gas velocities, the minimum D_b is observed when the apparent water velocity reaches 0.2265 m/s. This phenomenon can be interpreted as follows: under conditions of low water velocity, the turbulence within the liquid phase remains weak, resulting in limited kinetic energy transfer to the steel balls. Consequently, their shearing action on bubbles is insufficient, which leads to the formation of larger bubbles. As water velocity increases, the turbulence within the liquid phase intensifies, thereby boosting the kinetic energy of the steel balls. This heightened energy promotes more frequent and forceful interactions between the steel balls and bubbles within the mineralized zone, effectively breaking up the bubbles and causing D_b to decrease. The decline in D_b continues until it hits a minimum value.

However, when the apparent water velocity continues to rise, the liquid turbulence becomes excessive, increasing the porosity within the steel ball layer. This higher porosity reduces the frequency of steel ball collisions, thereby diminishing their capacity to shear bubbles. As a result, D_b begins to increase again, now more influenced by the turbulence of the fluid than by mechanical shear. Beyond a certain point, further increases in water velocity no longer significantly alter turbulence intensity, leading to a steady state in D_b where it becomes relatively constant due to the saturation of turbulence effects on bubble breakup.

3.1.4. Study of the effect of apparent gas velocity on bubble diameter

As illustrated in Fig. 7, the relationship between D_b and apparent gas velocity exhibits distinct trends depending on the level of apparent water velocity. At lower apparent water velocities (0.1698–0.1980 m/s), D_b demonstrates a negative correlation with increasing gas velocity. This behavior is primarily attributed to the relatively low turbulence intensity within the fluidized bed under such conditions. As the gas velocity increases, turbulence in the liquid phase intensifies accordingly. The combined influence of both fluid phases enhances the kinetic energy and shear interactions of the fluidized steel balls, promoting bubble breakup and thereby reducing D_b. These results are consistent with prior studies indicating that an increase in the gas phase under low water flow conditions can effectively reduce bubble size. Conversely, when the apparent water velocity exceeds 0.2265 m/s, D_b shows a slight positive correlation with apparent gas velocity. This weaker response is due to the already high turbulence intensity generated by the elevated water velocity, which limits the marginal contribution of the gas phase. Moreover, given the relatively narrow adjustment range of apparent gas velocity in this study, its effect on further enhancing turbulence is constrained. As a result, bubble breakup is less influenced by shear interactions, and the increase in gas velocity leads to a modest increase in D_b.

It is important to note that the influence of gas velocity on bubble size is governed by multiple factors, including turbulence regime, phase interaction, and system configuration, making the relationship inherently complex and system-specific. In the present work, the broader adjustment range for apparent water velocity, in contrast to the narrower gas velocity range, plays a key role. Under low water velocity conditions, the introduction of gas substantially enhances liquid-phase turbulence, which intensifies bubble–steel ball interactions and thus contributes to a reduction in D_b.

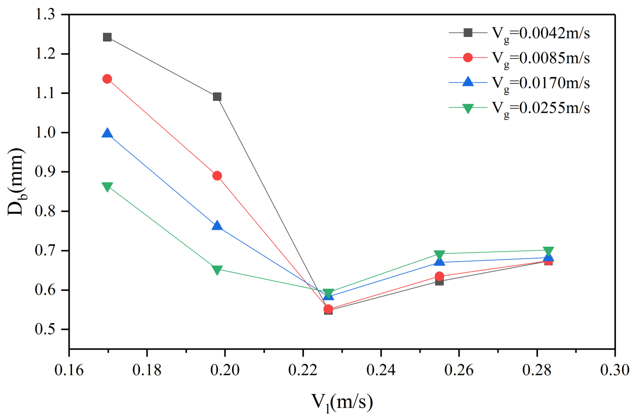

Fig. 6. Relationship between D_b and superficial liquid velocities

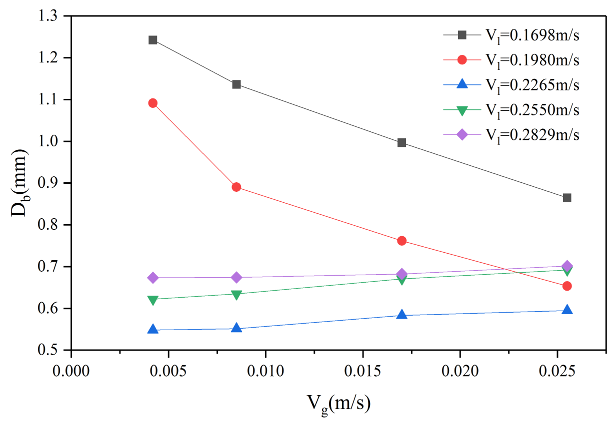

Fig. 7. Relationship between D_b and superficial gas velocities

3.2. Measurement and analysis of gas content ratio

Gas content is one of the key parameters to characterize the mass transfer process in a flotation column [87]. Theoretically, the higher the gas content and the better the bubble condition, the higher the flotation efficiency, so the gas content can reflect the performance index of the flotation unit from the side. In this section, the effects on the gas content ratio are mainly investigated by changing the apparent water velocity, apparent gas velocity, static bed height, and heavy phase mass ratio.

3.2.1. Effect of apparent gas velocity on gas content ratio

From Fig. 8, it can be clearly seen that for the same apparent water velocity, the gas content rate with the increase of apparent gas velocity has an increasing trend, for different apparent water velocity, the law of change is also the same. The reason for this law is that the gas content rate is most affected by the apparent gas velocity, the apparent increase in gas velocity is realized by increasing the gas flow rate, through the gas flow meter means that more gas flow rate per unit of time into the gas volume increased, at the same time, the D_b decreases so that the number of its increased, resulting in slower uplift, increasing the residence time of the bubbles in the bed, which led to the increase in the rate of the gas content rate. However, with the further increase of gas velocity, a large amount of gas produced a turbulent bubble flow, which intensified the interaction between the bubbles, and the bubble merger phenomenon was also strengthened, which led to the acceleration of the escape rate of the bubbles in the bed, thus resulting in the slowing down of the rate of increase of the gas content rate. However, the increase of gas inlet is the main factor to promote the increase of gas content rate, so after the apparent gas velocity reaches a certain value, the increase of gas content rate slows down but is still increasing.

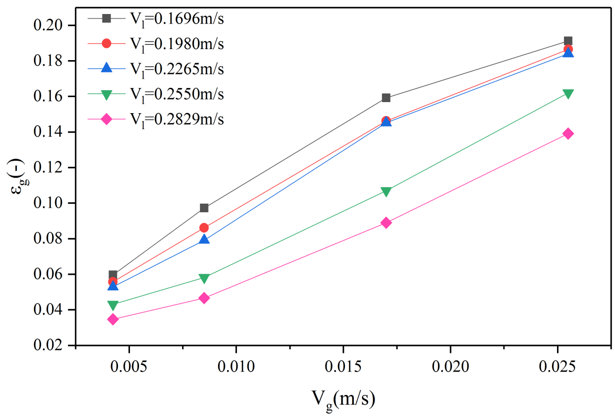

Fig. 8. Relationship between gas hold-up rate and superficial gas velocities

3.2.2. Effect of apparent water velocity on gas content ratio

Under conditions of a static bed height of 0.2885 m, the influence of apparent water velocity on the gas holdup ratio is depicted in Fig. 9. As observed in the figure, gas holdup consistently decreases with increasing apparent water velocity across all tested apparent gas velocities. This trend can be attributed to the enhanced buoyant force exerted on gas bubbles as water velocity increases. Specifically, higher apparent water velocities promote the upward transport of bubbles, effectively accelerating their escape from the mineralized bed region. As a result, the residence time of gas bubbles within the fluidized bed is reduced, thereby leading to a decline in overall gas holdup.

3.2.3. Effect of static bed height on gas content ratio

Fig. 10 shows the effect of increasing static bed height on gas content rate. It can be seen that the gas content rate increases with the increase of static bed height at all apparent gas velocities, and then increases gently or slightly. This phenomenon is mainly due to two reasons, one is that the filling steel ball has a shear effect on the bubbles, and the steel ball makes the large bubbles fully broken and increases the gas content; the other reason is that the bubbles wrapped in liquid will have a certain degree of adhesion on the surface of the bed layer steel ball, and the increase in the static bed layer height increases the probability of such adhesion, and the distribution of the gas bubbles in the residence time of the mineralized bed layer is increased, which makes the gas content rate become larger. However, after the height of the static bed layer increases to a certain height, the violent collision of the steel balls causes the bubbles adhering to the surface of the steel balls to fall off, so the increase of the gas content rate decreases, and at the same time, the shear crushing effect of the steel balls on the bubbles also reaches its maximum.

3.2.4. Effect of heavy phase mass ratio on gas content ratio

It can be seen from Fig. 11, in the static bed layer height of 0.2885m, the apparent water velocity of 0.2265m/s constant conditions, the gas content rate with the change of the heavy phase mass ratio is not obvious, in the heavy phase mass ratio of 50%, some of the larger, through the previous study can be known that at this time the minimum diameter of the bubbles, small bubbles of the uplift speed is slow, resulting in the prolongation of the retention time of the bubbles in the bed layer, and at the same time, the number of bubbles is also, so the gas content rate is increased accordingly.

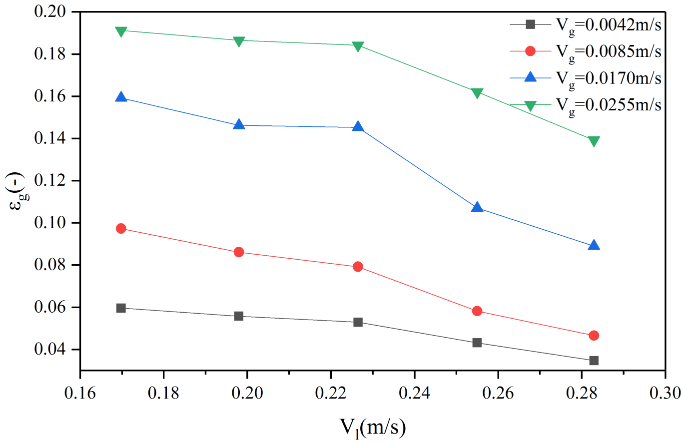

Fig. 9. Relationship between gas hold-up rate and superficial liquid velocities

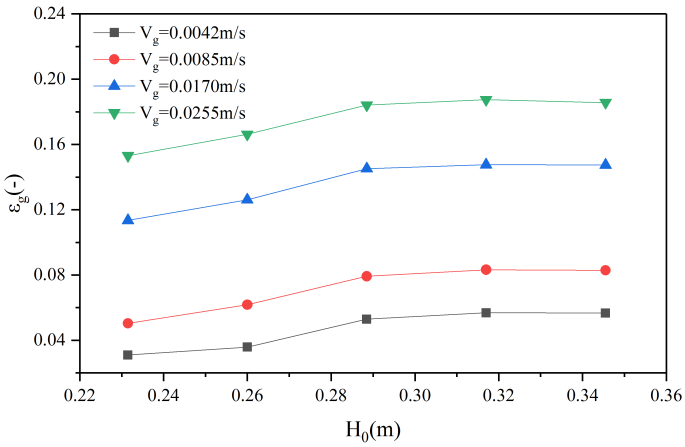

Fig. 10. Relationship between gas hold-up rate and static bed height

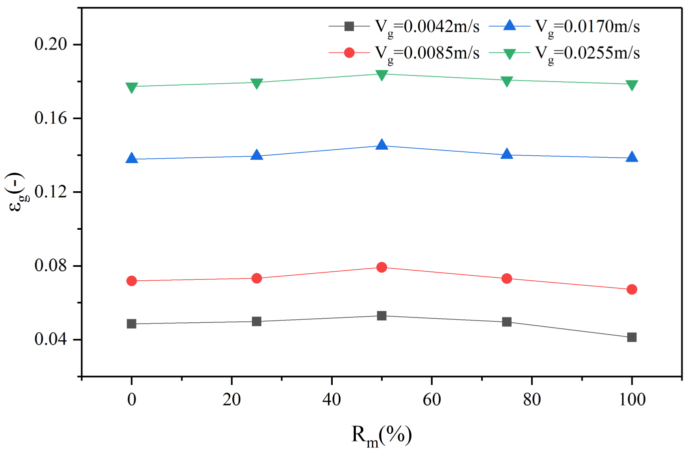

Fig. 11. Relationship between gas hold-up rate and heavy mass rate

3.3. Study on gas parameters by Box-Behnken response surface optimization

Through the analysis in the previous section, the effects of apparent water velocity, apparent gas velocity, static bed layer height and heavy phase mass ratio on the gas parameters of the fluidized bed flotation column can be determined, and in order to further explore the importance and correlation of the factors, the Box-Behnken response surface optimization (BBD) method is now selected for the experimental design through the Design-expert software, which is not only able to significantly reduce the This method not only can greatly reduce the amount of test, but also can fit the test data, statistical analysis, mathematical modeling, etc., using the obtained three-dimensional response surface map can be a comprehensive analysis of the interaction between multiple factors and the degree of influence. After determining a reasonable range of factor operation, the experimental design was carried out according to four factors and three levels, and the data were analyzed, fitted, and mathematical models were established, the experimental factors and levels are shown in Table 1, and the experimental results are shown in Table 2.

Table 1. Variable and levels of Box-Behnken Design

considerations	level (of achievement etc)		
	-1	0	1
A-apparent water velocity, m/s	0.1980	0.2265	0.2550
B-apparent gas velocity, m/s	0.0085	0.0170	0.0255
C-height of static bed layer, m	0.2600	0.2885	0.3170
D-heavy phase mass ratio, %	25	50	75

Table 2. Box-Behnken Design and corresponding results

serial number	A	B	C	D	ε_g	D_b
1	0.2265	0.0170	0.2885	50	0.1397	0.58
2	0.2265	0.0255	0.2885	25	0.1738	0.91
3	0.2550	0.0255	0.2885	50	0.1584	0.67
4	0.2265	0.0170	0.2600	25	0.0815	1.33
5	0.2265	0.0170	0.2885	50	0.1397	0.58
6	0.2265	0.0170	0.3170	75	0.1317	0.96
7	0.2265	0.0170	0.3170	25	0.1119	1.03
8	0.2265	0.0085	0.3170	50	0.0526	1.02
9	0.1980	0.0085	0.2885	50	0.0851	0.89
10	0.2550	0.0170	0.2600	50	0.0282	1.29
11	0.2265	0.0085	0.2885	75	0.0702	0.56
12	0.2265	0.0255	0.2885	75	0.1753	0.61
13	0.2265	0.0085	0.2885	25	0.0695	0.57
14	0.2550	0.0170	0.2885	25	0.1127	0.73
15	0.2550	0.0170	0.2885	75	0.1104	0.76
16	0.2265	0.0170	0.2885	50	0.1397	0.58
17	0.1980	0.0170	0.2885	25	0.1362	0.80
18	0.2265	0.0255	0.3170	50	0.1841	0.97
19	0.2265	0.0170	0.2885	50	0.1397	0.58
20	0.1980	0.0170	0.3170	50	0.1464	0.93
21	0.1980	0.0170	0.2885	75	0.1401	0.78
22	0.2550	0.0085	0.2885	50	0.0582	0.63
23	0.1980	0.0170	0.2600	50	0.0462	1.52
24	0.2265	0.0085	0.2600	50	0.0352	1.25
25	0.2265	0.0170	0.2600	75	0.1002	1.30
26	0.1980	0.0255	0.2885	50	0.1835	0.65
27	0.2265	0.0255	0.2600	50	0.1622	1.45
28	0.2265	0.0170	0.2885	50	0.1397	0.58
29	0.2550	0.0170	0.3170	50	0.1135	1.05

3.4. Study of factors affecting bubble diameter

Combining Table 3 and Table 4, it can be seen that the recommended model for the D_b is Quadratic, and its Prob value is less than 0.0001, which is much less than 0.05, indicating that its fit is high, and R^2 is greater than 0.9 proving that the model has higher correlation with the test, and that the model is more accurate, therefore, after analyzing the Quadratic model, we get Table 5, and it can be seen from the data in the table, the influence on the model The correlation factors and the order of magnitude are C, AC>AB, C^2>A^2, respectively. According to the significance of the degree of influence, the software then optimizes the insignificant terms to obtain the prediction model for D_b, which is represented by the actual factors of D_b and the relationship between the factors as follows:

$$D_b=70.165-97.739A+7.176B-398.061C-0.0039D+313.416AB+107.51AC+0.0161AD-261.92BC-0.342BD-0.0143CD+131.199A^2+534.487B^2+645.511C^2+0.000089D^2$$

Fig. 12 shows the normal distribution of the residual values of D_b prediction and the comparison between the test values and the predicted values, respectively. From the figure, it can be seen that the residual values show a more obvious linear distribution, and the deviation of the test values from the predicted values is not obvious, so that the mathematical model of D_b can be obtained to have very good predictive properties.

To analyze the effect of the other two factors and their interactions on D_b when two of the factors, apparent water velocity, apparent gas velocity, static bed height, and heavy phase mass ratio, are fixed, the values of the fixed factors are taken to be the intermediate of the levels of the factors taken, and the response surfaces are shown in Fig. 13, (a)-(f).

What can be seen from each graph in Fig. 13 is that the pattern of D_b influenced by single-factor variations is the same as the results of the single-factor analysis test in the previous section, and the degree of interaction between the factors can be seen from the steepness of the peaks of each response surface plot. From Fig. 13(a), it can be seen that the apparent water velocity interacts with the apparent gas velocity on the D_b, which also indicates the synergistic effect of the apparent gas velocity on the apparent water velocity to some extent. D_b is most affected by the static bed height (Fig. 13(b), (d), (f)), D_b decreases and then increases with the increase of the static bed height, and the bubble sot diameter

Table 3. Variety of models analysis of variance

Source of variance	square sum (e.g. equation of squares)	(number of) degrees of freedom (physics)	mean square	F-value	Prob>F	note
Mean vs Total	22.62	1	22.62			
Linear vs Mean	0.44	4	0.11	1.33	0.2872	
2FI vs Linear	0.092	6	0.015	0.15	0.9875	
Quadratic vs 2FI	1.82	4	0.45	97.39	< 0.0001	Suggested
Cubic vs Quadratic	0.058	8	7.285E-003	6.16	0.0199	Aliased
Residual	7.097E-003	6	1.183E-003			
Total	25.03	29	0.86			

Table 4. Comprehensive analysis of variance on multiple models

variance (statistics)	standard deviation	R^2	R^2 correction value	R^2 Predicted value	Predicting the residual sum of squares	note
Linear	0.29	0.1815	0.0451	-0.1904	2.87	
2FI	0.32	0.2195	-0.2141	-1.1721	5.25	
Quadratic	0.068	0.9729	0.9459	0.8440	0.38	Suggested
Cubic	0.034	0.9971	0.9863	0.5768	1.02	Aliased

Table 5. Variance analysis of Quadratic model

variance (statistics)	square sum (e.g. equation of squares)	(number of) degrees of freedom (physics)	mean square	F-value	Prob F>
Model	2.35	14	0.17	35.93	< 0.0001
A - Apparent water velocity	0.013	1	0.013	2.79	0.1171
B - Apparent gas velocity	0.012	1	0.012	2.50	0.1364
C - Height of static bed	0.40	1	0.40	85.97	< 0.0001
D-heavy phase mass ratio	0.012	1	0.012	2.62	0.1281
AB	0.023	1	0.023	4.94	0.0433
AC	0.031	1	0.031	6.53	0.0229
AD	5.267E-004	1	5.267E-004	0.11	0.7420
BC	0.016	1	0.016	3.45	0.0845
BD	0.021	1	0.021	4.53	0.0516
CD	4.162E-004	1	4.162E-004	0.089	0.7697
A2	0.074	1	0.074	15.77	0.0014
B2	9.673E-003	1	9.673E-003	2.07	0.1721
C2	1.78	1	1.78	381.86	< 0.0001
D2	0.020	1	0.020	4.28	0.0576
Residual	0.065	14	4.670E-003		
Lack of Fit	0.065	10	6.538E-003		
Pure Error	0.000	4	0.000		
Cor Total	2.41	28			

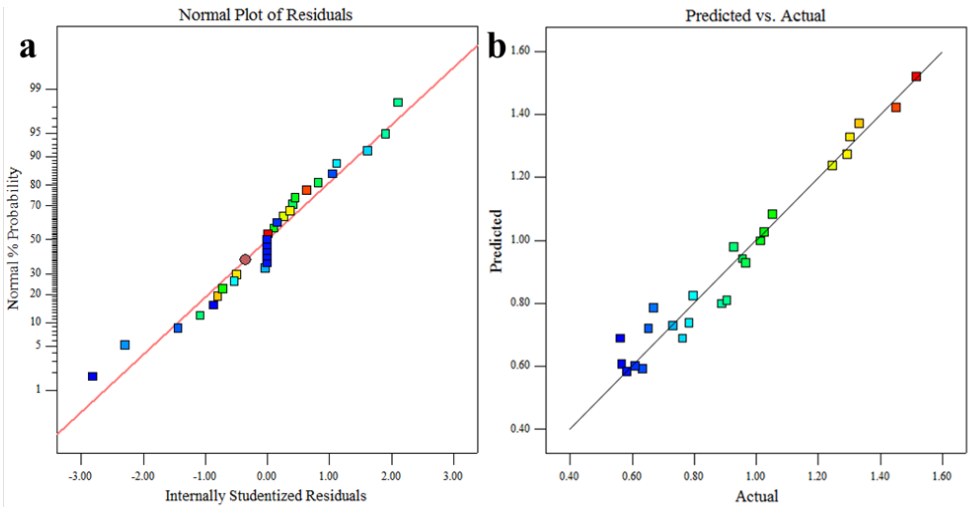

Fig. 12. a. Normal plot of residuals for predicting value of D_b. b. Comparison between predicting and experimental value of D_b

is the smallest at the initial static bed height of 0.2885 m. This is because with the increase of the static bed height, the bed steel beads enhance the shear force on the bubbles until this shear effect reaches the optimum, and then, due to the bed height too high leads to a longer bubble overflow time, which causes the bubbles to undergo merger behavior as they pass through the bed layer, thus leading to a larger D_b as they pass through the excessively high filled bed layer. As can be seen from the response surface plot in Fig. 13(d), the increase in apparent gas velocity when the static bed layer height changes has little effect on the change in D_b, which also further illustrates that the static bed layer height not only has a significant shear effect on the D_b, but also has a significant effect on the annexation behavior during the rise of the bed bubbles, and when the shear effect is dominant, the bed steel beads show a shear effect on the bubbles; on the contrary, when the initial stationary bed height exceeds a certain range, the annexation effect on bubbles will be stronger than the shear effect, but it can ensure the uniformity of bubbles in the case of larger gas velocity. From Fig. 13(c) and (e), it can be seen that the heavy-phase mass ratio interacts with the apparent water velocity and apparent gas velocity, respectively, which is because the shear effect of the steel balls on the bubbles is related to the mass of the steel balls themselves for different apparent water and gas velocities, and when the heavy-phase mass ratio is low, the higher apparent water velocity increases the porosity of the steel balls, and the steel balls do not have a strong shear effect on the bubbles, whereas in the case of a high heavy-phase mass ratio, the higher apparent The turbulence intensity generated by the water velocity makes the shearing effect of steel balls on the bubbles stronger, and the D_b is smaller than that of the case with a low heavy-phase-to-mass ratio. When the heavy-phase-to-mass ratio is 50%, the particle size ratio of the cross-section particles of the column is the largest at this time, and the steel balls have the strongest shearing effect on the bubbles, and therefore, D_b is also the smallest.

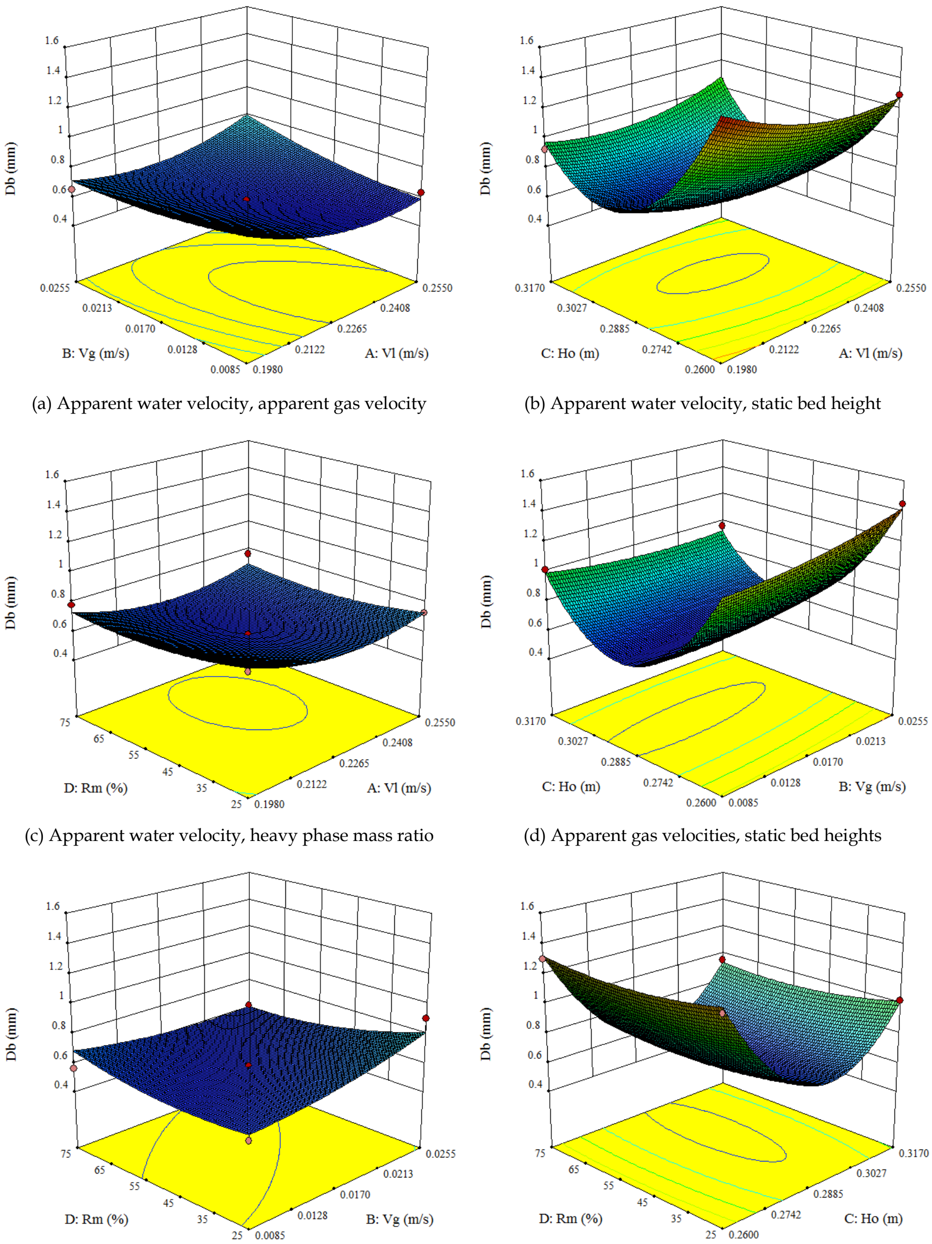

(a) Apparent water velocity, apparent gas velocity

(b) Apparent water velocity, static bed height

(c) Apparent water velocity, heavy phase mass ratio

(d) Apparent gas velocities, static bed heights

Fig. 13. Effect of the other two factors on the D_b when two factors are fixed

4. Conclusions

In this study, a one-factor analysis test was conducted to investigate the effects of changes in apparent water velocity, apparent gas velocity, static bed layer height and heavy phase mass ratio on D_b and gas content, and then a four-factor, three-level test was designed using the BBD optimization method to determine the significance of the four factors, namely, apparent water velocity, apparent gas velocity, static bed layer height and heavy phase mass ratio, as well as the effects of the interactions of the four factors on the D_b and gas content, respectively. gas content, and the prediction models of D_b and gas content were determined, and the following conclusions were drawn:

(1) Fluidized bed flotation column D_b study shows that the appropriate static bed height has an important effect on the production of small D_b, the D_b reduction has a significant shear effect, in the static bed height reaches a certain value, this effect will be weakened; the increase in the heavy-phase mass ratio of D_b reduction has a certain effect on the particles, particle size ratio changes, the two particles fill each other with fluidized interstitials, in the heavy phase mass ratio of 50%, the shear effect on the bubble reaches the optimum, so D_b is the smallest at this time; the increase of apparent water velocity has a more significant effect on the D_b, in the apparent water velocity of 0.2265m/s, D_b is the smallest, more than this water velocity, D_b has a tendency to gradually increase, but the follow-up is more gentle; the apparent air velocity on D_b has a different influence on the law, in the low apparent water velocity, the The increase of apparent air velocity decreases D_b, while the effect of apparent air velocity on D_b is not significant when the apparent water velocity is greater than 0.2265 m/s.

(2) It is found that the increase of apparent gas velocity has the most significant effect on the increase of gas content, i.e., the larger the apparent gas velocity is, the larger the gas content is; the apparent water velocity has a side effect on the gas content, i.e., the increase of apparent water velocity gradually decreases the gas content; the increase of the static bed height helps to increase the gas content, but after the bed height is more than 0.2885 m, the increase of the bed height has a significant decrease in the increase of the gas content; the effect of the heavy-phase mass ratio on the gas content is not obvious. The effect of heavy phase mass ratio on the gas content ratio is not obvious, and the gas content ratio has the maximum value when the value is 50%.

(3) Box-Behnken response surface optimization method of gas parameters showed that the influence of the factors on D_b and gas content rate of the law is consistent with the previous single-factor test obtained law, for the D_b, the relevant factors and the size of the order of the influence of the model are: C, AC>AB, C^2>A^2, and get the prediction model for:

$$D_b=70.165-97.739A+7.176B-398.061C-0.0039D+313.416AB+107.51AC+0.0161AD-261.92BC-0.342BD-0.0143CD+131.199A^2+534.487B^2+645.511C^2+0.000089D^2$$

Acknowledgments

This work was supported by National Natural Science Foundation of China (No.51674258).

References

ABU, K., MADHURANTHAKAM, C., DHIB, R., 2021. *Empirical models for the hydrodynamics of turbulent bed contactor with non-Newtonian liquids. (part 3).* Chem. Eng. Commun. 208(1), 110–125.

AOYAMA, S., HAYASHI, K., HOSOKAWA, S., TOMIYAMA, A., 2016. *Shapes of ellipsoidal bubbles in infinite stagnant liquids.* Int. J. Multiph. Flow. 79, 23–30.

BESAGNI, G., INZOLI, F., 2019. *Bubble sizes and shapes in a counter-current bubble column with pure and binary liquid phases.* Flow Meas. Instrum. 67, 55–82.

BHUNIA, K., KUNDU, G., MUKHERJEE, D., 2015. *Statistical model for gas holdup in flotation column in presence of minerals.* Can. Metall. Q. 54(2), 235–246.

CAI, X., CHEN, J., LIU, M., JI, Y., AN, S., 2017. *Numerical studies on dynamic characteristics of oil-water separation in loop flotation column using a population balance model.* Sep. Purif. Technol. 176, 134–144.

ELLINGSEN, K., RISSO, F., 2001. *On the rise of an ellipsoidal bubble in water: oscillatory paths and liquid-induced velocity.* J. Fluid Mech. 440, 235–268.

FAN, M., TAO, D., ZHAO, Y., HONAKER, R., 2013. *Effect of nanobubbles on the flotation of different sizes of coal particle.* Miner. Metall. Process. 30(3), 157–161.

GORAIN, B., FRANZIDIS, J., MANLAPIG, E., 1999. *The empirical prediction of bubble surface area flux in mechanical flotation cells from cell design and operating data.* Miner. Eng. 12(3), 309–322.

JENA, H., ROY, G., MEIKAP, B., 2008a. *Prediction of gas holdup in a three-phase fluidized bed from bed pressure drop measurement.* Chem. Eng. Res. Des. 86(11A), 1301–1308.

JENA, H., SAHOO, B., ROY, G., MEIKAP, B., 2008b. *Characterization of hydrodynamic properties of a gas-liquid-solid three-phase fluidized bed with regular shape spherical glass bead particles.* Chem. Eng. J. 145(1), 50–56.

JO, Y., PARK, S., YOO, H., KIM, E., 2022. *GPU-based SPH-DEM Method to Examine the Three-Phase Hydrodynamic Interactions between Multiphase Flow and Solid Particles.* Int. J. Multiph. Flow 153.

LEFEBVRE, S., GUY, C., CHAOUKI, J., 2007. *Solid phase hydrodynamics of three-phase fluidized beds - A convective/dispersive mixing model.* Chem. Eng. J. 133(1–3), 85–95.

LEI, W., ZHANG, M., ZHANG, Z., ZHAN, N., FAN, R., 2020. *Effect of bulk nanobubbles on the entrainment of kaolinite particles in flotation.* Powder Technol. 362, 84–89.

LI, Y., LI, Q., YANG, J., ZHOU, X., YIN, X., ZHAO, D., 2008. *Expression patterns of Doppel gene in golden hamster: Quantification using real-time RT-PCR.* Mol. Cell. Probes. 22(4), 255–258.

LIU, L., ZHANG, H., YAN, H., ZIEGENHEIN, T., HESSENKEMPER, H., ZHOU, P., LUCAS, D., 2021. *Experimental studies on bubble aspect ratio and corresponding correlations under bubble swarm condition.* Chem. Eng. Sci. 236.

LOTH, E., 2008. *Quasi-steady shape and drag of deformable bubbles and drops.* Int. J. Multiph. Flow 34(6), 523–546.

PAN, H., LI, Y., LI, N., GAO, F., FU, X., ZHU, R., EVANS, G., 2018. *Study on gas holdup in a fluidized flotation column from bed pressure drop. Energy Sources A: Recovery Util. Environ.* Eff. 40(14), 1693–1700.

RAVICHANDRAN, V., ESWARAIH, C., SAKTHIVEL, R., BISWAL, S., MANISANKAR, P., 2013. *Gas dispersion characteristics of flotation reagents.* Powder Technol. 235, 329–335.

SARHAN, A., NASER, J., BROOKS, G., 2017. *CFD analysis of solid particles properties effect in three-phase flotation column.* Sep. Purif. Technol. 185, 1–9.

SHI, W., YANG, J., LI, G., YANG, X., ZONG, Y., CAI, X., 2018. *Modelling of breakage rate and bubble size distribution in bubble columns accounting for bubble shape variations.* Chem. Eng. Sci. 187, 391–405.

SOBRINO, C., ALMENDROS-IBÁÑEZ, J., SANTANA, D., VÁZQUEZ, C., DEVEGA, M., 2009. *Maximum entropy estimation of the bubble size distribution in fluidized beds.* Chem. Eng. Sci. 64(10), 2307–2319.

VADLAKONDA, B., MANGADODDY, N., 2018. *Hydrodynamic study of three-phase flow in column flotation using electrical resistance tomography coupled with pressure transducers.* Sep. Purif. Technol. 203, 274–288.

VENKATRAMAN, P.Z., 1996. *Evaluation of an advanced fine coal cleaning circuit*.

WANG, G., GE, L., MITRA, S., EVANS, G., JOSHI, J., CHEN, S., 2018. *A review of CFD modelling studies on the flotation process.* Miner. Eng. 127, 153–177.

WANG, T., WANG, J., YANG, W., JIN, Y., 2003. *Experimental study on bubble behavior in gas-liquid-solid three-phase circulating fluidized beds.* Powder Technol. 137(1–2), 83–90.

YIANATOS, J., VINNETT, L., PANIRE, I., ALVAREZ-SILVA, M., DÍAZ, F., 2017. *Residence time distribution measurements and modelling in industrial flotation columns.* Miner. Eng. 110, 139–144.